

Deep Space *Ka*-Band Link Management and Mars Reconnaissance Orbiter: Long-Term Weather Statistics Versus Forecasting

FARAMAZ DAVARIAN, SHERVIN SHAMBAYATI, AND STEPHEN SLOBIN

Contributed Paper

During the last 40 years, deep space radio communication systems have experienced a move toward shorter wavelengths. In the 1960s, a transition from L- to S-band occurred, which was followed by a transition from S- to X-band in the 1970s. Both these transitions provided deep space links with wider bandwidths and improved radio metrics capability. Now, in the 2000s, a new change is taking place: namely, a move to the *Ka*-band region of the radio frequency spectrum.

Ka-band will soon replace X-band as the frequency of choice for deep space communications, providing ample spectrum for the high data rate requirements of future missions. The low-noise receivers of deep space networks have a great need for link management techniques that can mitigate weather effects. In this paper, three approaches for managing *Ka*-band Earth-space links are investigated. The first approach uses aggregate annual statistics, the second one uses monthly statistics, and the third is based on the short-term forecasting of the local weather. An example of weather forecasting for *Ka*-band link performance prediction is presented. Furthermore, spacecraft commanding schemes suitable for *Ka*-band link management are investigated.

These schemes will be demonstrated using NASA's Mars Reconnaissance Orbiter spacecraft in the 2007–2008 period, and the demonstration findings will be reported in a future publication.

Keywords—Atmospheric noise temperature forecasting, deep space link management, *Ka*-band link design, satellite communications, weather effects on radio signals.

I. INTRODUCTION

The exploration of the solar system with spacecraft and/or scientific probes has evolved since its early days in the 1960s. Unmanned probes are reaching deeper into space and are generating more science data to be sent back to

Manuscript received June 1, 2004; revised August 31, 2004. This work was carried out at the Jet Propulsion Laboratory, California Institute of Technology, Pasadena, under a contract with the National Aeronautics and Space Administration.

The authors are with the Jet Propulsion Laboratory, California Institute of Technology, Pasadena, CA 91109 USA (e-mail: Davarian@jpl.nasa.gov; Shervin.Shambayati@jpl.nasa.gov; Stephen.D.Slobin@jpl.nasa.gov).

Digital Object Identifier 10.1109/JPROC.2004.837613

Sky Noise Temperature (K) due to Oxygen

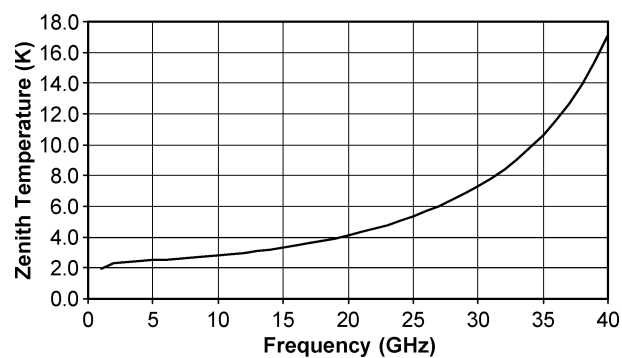


Fig. 1. The minimum zenith sky noise temperature.

Earth. Whereas in the early days spacecraft were designed to transmit at a rate of a few kilobits per second from planetary distances, future missions expect transmission rates of about 1 Mb/s or more [1]. Therefore, deep space systems need to evolve to keep pace with the increasing demands.

Deep space links are distinguished from their near-Earth counterparts in that deep space signals are likely to be very weak and, therefore, they cannot be detected with conventional commercial receiving systems. A main characteristic of deep space receivers is their unconventional low-noise requirement. While commercial near-Earth *Ka*-band receivers employ low-noise systems with noise temperatures of about 150 K, deep space systems employ receivers with much lower noise temperatures of approximately 25 K.¹ The very low noise property of deep space receiving systems makes them more sensitive to atmospheric effects than their commercial counterparts.

To a first-order approximation, Earth's troposphere is transparent to frequencies below about 1 GHz. For frequencies above about 1 GHz, atmospheric losses cannot be ignored, and these losses generally grow with increased frequency [2]. Furthermore, any lossy medium will emit

¹<http://deepspace.jpl.nasa.gov/dsdocs/810-005/>

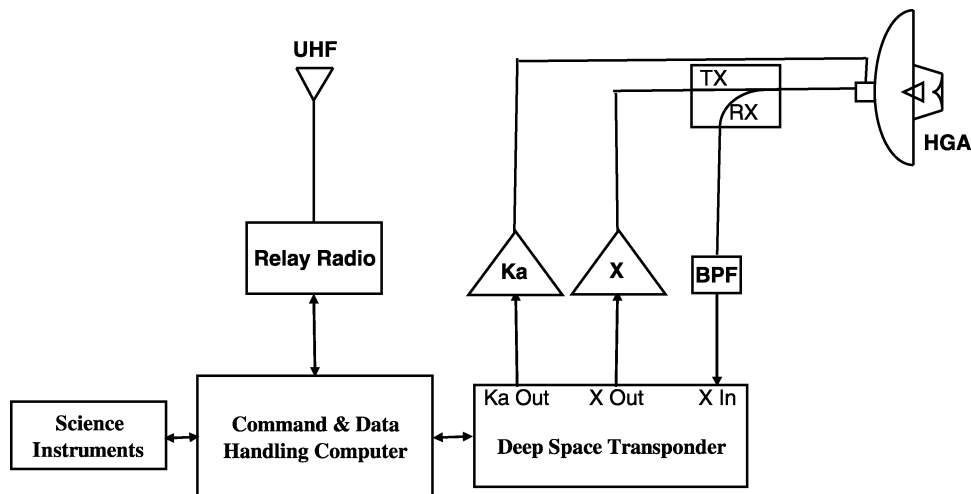


Fig. 2. MRO telecommunications and commanding subsystem.

radiation (noise) at all microwave frequencies, and the strength of this emission is dependent on both the loss and the physical temperature of the medium. Fig. 1 shows the minimum zenith noise temperature at sea level as a function of frequency for the range of 1–40 GHz. From this figure, it is clear that the minimum atmospheric noise temperature, which is caused solely by oxygen absorption, is negligible for *L*-band (less than 2 K at 1 GHz) and nontrivial for *Ka*-band (8 K at 32 GHz).

In practice, the atmosphere also contains a time-varying quantity of moisture in the form of water vapor and clouds. The amount of moisture depends on location, season, and time of day. In addition, hydrometeors in the form of rain, hail, and snow can also be present with a lower probability than water vapor and clouds. A special issue of the PROCEEDINGS OF THE IEEE provides data and discussions on the effect of Earth's atmosphere on *Ka*-band signals [3].

Due to the probabilistic nature of the losses associated with the atmosphere at frequencies above about 1 GHz, it is generally difficult to design a link that is reliable and conserves system resources. As will be shown later in this paper, for frequencies below about 10 GHz, atmospheric losses may be mitigated by the allocation of a constant margin. But this approach for frequencies above about 10 GHz does not yield desirable results. In this paper, two frequencies of interest, 8.4 GHz (*X*-band) and 32 GHz (*Ka*-band), will be discussed. The reason for this is that the deep space service has a 50-MHz allocation from 8.40 to 8.45 GHz (*X*-band) and a 500-MHz allocation from 31.80 to 32.30 GHz (*Ka*-band) [4].

Three approaches to *Ka*-band link management will be presented. These approaches will be tested by NASA's Mars Reconnaissance Orbiter (MRO) mission using Mars–Earth paths.

II. MRO MISSION

NASA's MRO is scheduled for launch in August 2005. The three phases of cruise, orbit insertion, and aerobraking

will take more than one year. The Mars orbiting spacecraft will begin its primary mission in November 2006. There are a number of sensors and a radar system onboard the spacecraft conducting high-resolution imagery, atmospheric science investigations, subsurface remote sensing, and other scientific observations. The primary mission is scheduled for two years, followed by a two-year period when the spacecraft will be used as a relay station between Mars probes and Earth [5].

Of interest in this paper is the telecom equipment onboard the orbiter. The MRO spacecraft will transmit at *X*- and *Ka*-bands, but it can only receive commands at *X*-band. The maximum aggregate downlink symbol rate that the spacecraft can support is 6 megasymbols/s. This rate is greater than any deep space mission before it. In addition to the high-rate satellite-to-Earth link, the telecom system supports a host of radio metrics including Doppler, ranging, and very long baseline interferometry (VLBI). It uses a 3-m, dual-frequency, high-gain antenna (HGA) with power amplifiers that provide the antenna with 35 W of *Ka*-band power and 100 W of *X*-band power. The spacecraft is also equipped with a relay telecom system for relaying data between Mars probes and Earth. The relay radio has its own separate antenna and power amplifier and operates at UHF frequencies. Fig. 2 shows the block diagram of the telecommunications and command subsystem of the spacecraft.

The telecom downlink can be configured in several ways, including suppressed carrier and residual carrier signaling. For forward error correction coding, two options of turbo codes and Reed–Solomon codes exist. The Reed–Solomon code can be concatenated with (7,1/2) convolutional code, and turbo codes offer a range of code rates and block sizes. Each of these selections will have an impact on the link performance. Although two options of quaternary phase-shift keying (QPSK) and binary phase-shift keying (BPSK) exist for data modulation, the *Ka*-band link will mostly employ the BPSK option for the demonstration. Assuming all other parameters have been selected, the data rate can be varied to increase or decrease the power margin of the link.

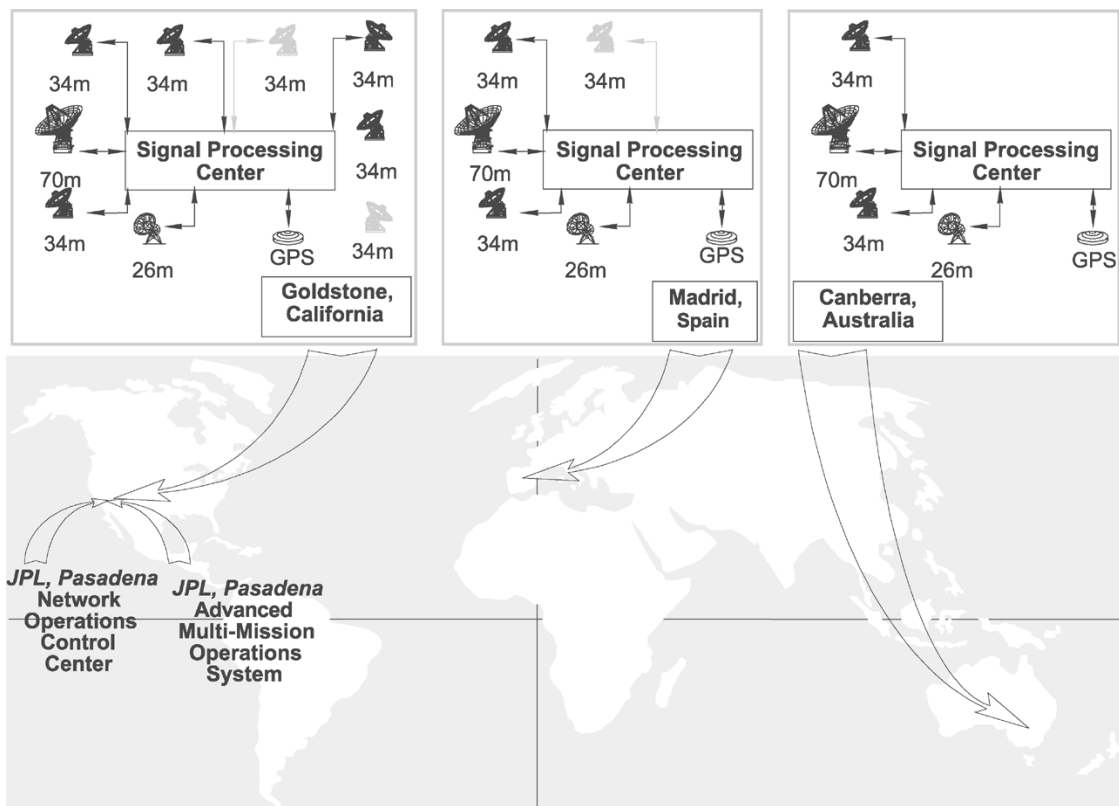


Fig. 3. DSN.

The standard method of commanding the spacecraft in deep space applications is to perform “background sequencing.” With this approach, the spacecraft is commanded once per month to reconfigure its parameters—particularly the telecom parameters of interest in this paper. The spacecraft configuration remains unchanged for one month until the next command arrives. In practice, once a month, the downlink transmission rate profiles for each of the next month’s passes are calculated and are uplinked to the spacecraft via background sequencing along with other telecom parameters. The background sequence will also contain nontelecom commands, including those that control the science instruments and those that are used for spacecraft navigation, orbital corrections, and routine maintenance.

III. DEEP SPACE NETWORK

The primary purpose of a deep space network is to provide communication and navigation services for deep space exploration. Communication takes place between a deep space asset (e.g., spacecraft, probe, etc.) and Earth. The uplink channel is used to transmit commands to the asset, and the downlink channel is used to transmit command verification, engineering data, and science data to Earth. Several nations operate deep space networks to support solar system exploration programs, notably, the United States, Russia, Japan, and a multitude of European nations represented by the European Space Agency. Because the U.S. deep space network will be used for communicating with the MRO spacecraft, a brief description of this network

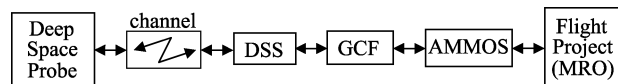


Fig. 4. End-to-end flow of command and telemetry between deep space probes and the flight projects. DSS: Deep Space Station; GCF: Ground Communications Facility; AMMOS: Advanced Multi-Mission Operation System.

will be given in this section. Furthermore, in this paper, the term “Deep Space Network (DSN)” will refer to the U.S. network funded by the National Aeronautics and Space Administration (NASA) and managed by the Jet Propulsion Laboratory (JPL) of the California Institute of Technology (Caltech), Pasadena.

The DSN consists of three sites (also known as complexes): Goldstone, CA (United States), Madrid (Spain), and Canberra (Australia).² These sites are spaced longitudinally about equally around the globe so that probes far from Earth are always in view of at least one complex. Each complex consists of a host of antennas with antenna diameter sizes of 70, 34, and 26 m. Recently some of the 34-m beam waveguide (BWG) antennas have become, or shortly will be, *Ka*-band capable. The combination of a particular antenna and its associated subsystems is referred to as a Deep Space Station (DSS). Fig. 3 shows the DSN site locations and their hardware.

Communications between Earth and space are classified as one of two processes: the uplink process that generates

²<http://deepspace.jpl.nasa.gov/dsndocs/810-005/>

Contribution of Atmospheric Noise Temperature to G/T at 30 Degrees Elevation for X-band and Ka-band vs. % Weather, Madrid

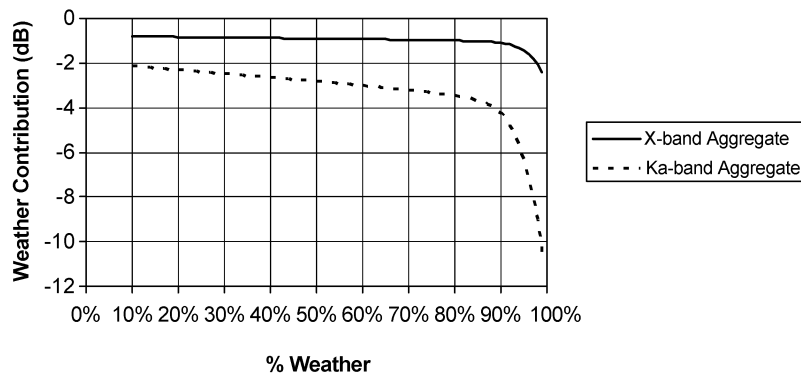


Fig. 5. Annual CDF of G/T losses due to weather; 34-m BWG antenna station at an elevation angle of 30°.

and transmits commands to the spacecraft, and the down-link process also known as telemetry. The DSN is an integral part of both these communications processes. In the uplink process, commands are generated by the flight project (MRO in this case). Then they are processed by the Advanced Multi-Mission Operation System (AMMOS) at JPL and relayed by the ground communication facility (GCF) to the DSN for transmission to the spacecraft. Similarly, telemetry (down-link) is received by DSN antennas, relayed over the GCF to AMMOS for processing, and sent to the flight project. DSN operations and scheduling are handled by the Network Operations and Control Center (NOCC) at JPL. Fig. 4 shows the end-to-end data flow between a deep space probe and its flight project.

IV. LINK VARIABILITY DUE TO WEATHER

The main challenge in determining *Ka*-band link parameters is the weather-induced uncertainty (variability) at the receiving station. As indicated in Section I, signal propagation through the atmosphere is subject to the dual effects of signal loss and increased receiving system noise temperature. Also, it should be noted that the levels of these effects are random and that they are both location and time dependent. The two effects of signal loss and system noise increase can jointly be described as they affect the link G/T. Signal loss reduces the apparent antenna gain *G*, whereas radio noise increases system noise temperature *T*. The result is a reduction of G/T due to weather. Clearly, this reduction is also a function of the path elevation angle. Usually the lowest G/T loss is associated with zenith (elevation angle of 90°), and the loss is increased as the elevation angle is reduced, approximately as to the inverse of the sine of the elevation.

Fig. 5 shows the expected G/T variation (relative to a “vacuum,” no-atmosphere condition) as a function of weather percentage obtained from long term radiometric observations at the Madrid complex. Ten years of radiometric data were accumulated for this figure. These statistics are known as the cumulative distribution function (CDF) of the G/T losses due to weather.

Note that, for example, loss L_{90} associated with the 90% point on the abscissa implies that 90% of the time the G/T loss is less than or equal to L_{90} . The 0% corresponds to the loss due to oxygen only. In Fig. 5, lower percentages correspond to good weather (clear) episodes; high percentages correspond to bad weather (stormy); and mid-level percentages correspond to intermediate weather. A few noteworthy observations are possible from Fig. 5.

- 1) By selecting a long term availability level in percentage on the abscissa, the required weather margin can be obtained from the vertical axis. For example if we desire a link availability of 95%, we need to provide 1.5 dB of atmospheric margin at *X*-band and 6 dB at *Ka*-band.
- 2) The minimum G/T loss, which is due to oxygen, for the Madrid 34-m BWG antenna station at an elevation angle of 30° is about 0.8 dB for *X*-band and about 2 dB for *Ka*-band.
- 3) If we define a good weather day as the percentage level of 20% and a bad weather day as the percentage level of 95%, we see that the difference in G/T losses between good and bad days is approximately 0.6 dB for *X*-band and 4 dB for *Ka*-band.

From 3) above, one can argue that since the link variability associated with *X*-band is only about 0.6 dB, there is not a strong incentive for trying to reduce the variability level by distinguishing between good and bad weather periods (day, month, season, etc.). But for *Ka*-band, the situation is different because the uncertainty of 4 dB is substantial. This uncertainty can be reduced by using a shorter time scale than yearly averages—for example, using monthly statistics rather than yearly. Therefore, whereas the use of the annual CDF can be recommended for the operation of *X*-band links, it is not recommended for the operation of *Ka*-band links.

The optimum transmission profile for each observing period not only depends on the meteorological history of the site during that period (for example, dry versus wet), it also depends on path range, elevation angle, and other relevant link parameters. Note that the optimum transmission profile is likely to vary from pass to pass, where a pass is defined as

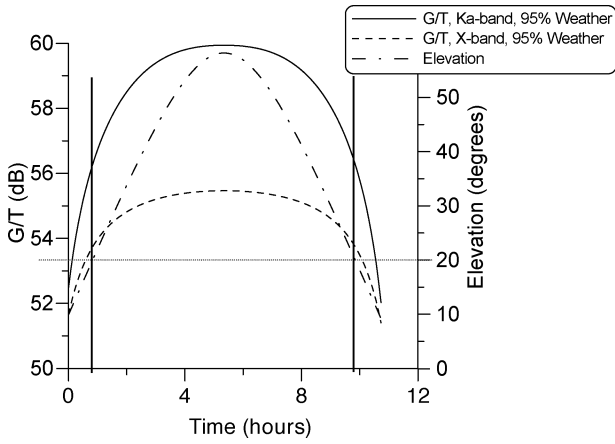


Fig. 6. Madrid receiver G/T and path elevation angle in the presence of Earth's atmosphere for the 34-m BWG antenna. The period for which elevation angle is above 20° is between the vertical lines.

an opportunity to observe the spacecraft at the site of interest, typically for at least a few hours.

A. Effect of Elevation Angle

As indicated earlier, the atmospheric loss increases with reduced elevation angle. Fig. 6 shows the G/T variation over a sample pass at the Madrid station at a time percentage level of 95%. The abscissa represents time, and the ordinate represents the G/T ratio. The middle curve shows the path elevation angle, corresponding to the right-hand ordinate in degrees. It is assumed that the link will operate over elevation angles equal to or greater than 20° —marked by vertical lines.

Noting Fig. 6, the G/T variation over the pass is approximately 2 dB for X-band and approximately 4 dB for Ka-band. This means that in the middle of the pass, the link can support a higher data rate than it can at the beginning and the end of the pass. It can be argued that while the potential data rate increase during the middle of the pass for X-band may not be worth the added complexity of multirate operations, for Ka-band the potential data rate increase of approximately 4 dB would justify multirate operations. Indeed, for Ka-band, nearly half of the pass has a G/T ratio of 3 dB or greater than the G/T at the beginning of the pass. In Section VII, it will be shown that good results can be obtained from the use of a simple two-rate system, where a lower transmission rate is used at low elevation angles and a higher rate is employed for high elevation angles during a pass.

One should note that there is a small penalty associated with a rate change, since the ground receiver needs time to re-lock onto the signal. This includes carrier, symbol, and frame synchronization times. Berner *et al.* [6] have proposed spacecraft bit-rate change in small steps to prevent the ground station from losing lock.

B. Deep Space Link Management Using Annual CDF of G/T

The use of the annual G/T CDF has been the convention for managing X-band links for the deep space service. Since the

weather-induced variation is relatively small at X-band, the CDF at the desired elevation angle can be used to determine the weather margin for the site of interest. In this fashion, the allotted budget for weather is likely to remain fixed, independent of season and elevation angle.

For Ka-band, however, this approach is not recommended. The allotted weather loss budget for Ka-band should depend on the season as well as the path elevation angle. The next section presents an approach that is suitable for managing Ka-band links.

V. LINK BUDGET DETERMINATION BASED ON THE MONTHLY CDF

In the previous section, it was shown that the annual statistics do not provide an efficient tool for the budgeting of the weather-induced losses in Ka-band links. Clearly, seasonal characterization of the atmospheric behavior will yield less uncertainty than annual characterization. In practice, depending on the site location and its weather characteristics, the CDF based on the season, month, or some other period may provide a good choice for estimating the required weather margin. In this section, monthly G/T statistics will be discussed.

Madrid station monthly CDFs relative to a no-atmosphere condition for the three months of April, July, and October are given in Fig. 7. This figure also contains the annual CDF for the same location, shown by the solid curve. The month-to-month variability of the Ka-band link G/T is evident.

It is observed that the link variability between good and bad weather events differs greatly from month to month. For example, July, being a relatively dry month at the Madrid station, has a small variability between a good day and a bad day. Again we compute variability as the difference between 20% and 95% levels. For July, this variability is about 1 dB, whereas the variability for October, a wet month, is 6 dB. Hence, the link uncertainty can be mitigated by using 1 dB of additional margin for July and 6 dB of additional margin for October.

From Fig. 7, it is evident that the annual CDF approximately matches April (a month that roughly represents the average weather in Madrid), but it does not match the characteristics of the dry nor the wet months. The aggregate CDF overestimates the dry month behavior and underestimates the wet month behavior. Therefore, if the annual CDF is used for link budget calculation, too much margin is applied to the link in July and not enough margin is provided in October. Hence, for improved performance, the link margin should be calculated from individual monthly CDFs rather than the aggregate yearly CDF. Section VII will present the performance of the link employing the monthly statistics.

The above scheme is based on monthly CDFs that have been constructed from multiyear radiometric observations at the site of interest. Assuming adequate historical data are available, the CDF represents stable statistics. Therefore, the average atmospheric margin for the month of interest can be calculated in advance. As noted in Section IV, the standard method of spacecraft commanding, known as background

**Weather Contributions to Ka-band G/T at 30 degrees Elevation vs. %
Weather for Different Atmospheric Noise Temperature Distributions, 34-m
BWG Antenna, Madrid**

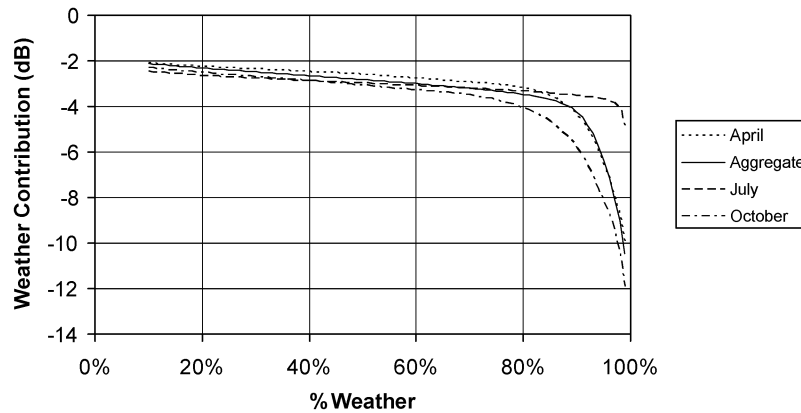


Fig. 7. Month-to-month variability of the *Ka*-band link is illustrated by comparing G/T monthly CDFs.

sequencing, is performed once a month. The scheme using monthly CDFs can be employed to set the telecom parameters of the spacecraft once per month. The data rate profile, modulation index profile, and coding profile are among parameters that will be reconfigured each month.

It is useful to note that variations on the above scheme are also possible. The selected time durations do not have to be of equal length. For example, during the summer, seasonal statistics can be used, whereas, for the rest of the year, monthly statistics can be employed.

It is also possible to have more than one CDF describing a period. For example, daytime statistics can be kept separate from nighttime statistics. This means that a different margin is calculated for the daytime operations versus the nighttime operations. Again note that the daytime and night periods do not have to be equal. For example, one can define daytime from local 8 A.M. to 4 P.M. and nighttime from 4 P.M. to 8 A.M.

VI. UNCERTAINTY REDUCTION VIA FORECASTING

Section IV showed that the main challenge in determining *Ka*-band link parameters is the weather-induced uncertainty at the receiving station. Section V demonstrated that the use of monthly statistics rather than yearly statistics lessens the amount of weather-induced uncertainty in the link. For example, at the Madrid site, knowing that July is a dry month (statistically speaking), the link is budgeted with a smaller margin than the yearly average margin. Similarly, knowing that October is a wet month, the link is budgeted with a margin higher than the yearly average.

Although the approach introduced in Section V clearly enhances the overall performance, it still leaves room for improvement. It can be argued that October, the wet month, is likely to have some dry periods. Hence, the excessive margin applied to that month is wasted during dry periods. Likewise, it can be argued that the lower than average margin applied to July, the dry month, will not protect the link in the event

of a storm. Therefore, it can be concluded that a shorter period than a month should be used for margin determination to further improve performance.

In Section V, the link atmospheric margin was determined for each month based on long-term monthly averages. The reader should note that the concept of a “month” here does not necessarily refer to a 30-day period. To be exact, this word is referring to any period that the days within that period have approximately the same statistics. Therefore, since all days in a month have the same weather-induced statistics, reducing the period of interest from one month to a shorter duration—for example, one day—would not improve the estimate. All days in a month have approximately the same mean value of the weather-related loss that is approximately equal to the monthly average. In summary, to improve performance above and beyond what was offered in Section V, a technique different from the use of historical statistics needs to be developed.

Weather forecasting can be used to predict the link behavior for a short time segment. Conceptually speaking, the coherence time of the local weather process should provide a good choice as the desired period—coherence time is defined as the period that, on the average, the local weather remains approximately unchanged. In this approach, each period is treated independent of the other periods. Since the behavior of the link is being observed over a short period relative to a month, the link uncertainty is further reduced. The next section provides an example of a weather forecasting technique that employs 6-h periods for forecasting, i.e., the coherence time is assumed to be 6 h.

A. Weather Forecasting

This section describes the weather forecasting mechanism that will be used as a part of the MRO demonstration. It should be noted that this approach reflects the current plan, and adjustments to this plan may take place by the onset of the demonstration in November 2006.

Since January 2002, the DSN has been receiving daily weather forecasts for the Goldstone site in the Mojave Desert of southern California. These forecasts are generated by the Spaceflight Meteorology Group (SMG) of the National Weather Service located at Johnson Space Center in Houston, TX.³ The primary responsibility of SMG is to provide weather support for space shuttle operations, including weather forecasts for emergency landing locations. The forecasted weather is turned into forecasts of atmospheric noise temperature and attenuation for use in modeling telecommunications links, i.e., predicting G/T, so as to maximize data return, consistent with acceptable continuity of the data.

Forecasts are received daily and consist of specific atmospheric descriptions beginning 12 h in the future (12 h from the data set upon which the forecast is based), out to 120 h in the future, at 6-h intervals. The complete daily forecast set consists of 19 individual forecasts. Strictly speaking, the forecast is considered valid only for the instant of time specified, but for the purposes of noise temperature forecasting, the forecast is considered valid for a 6-h period beginning 3 h before the valid time until 3 h after the valid time. Thus, the total valid time covered is from 9 to 123 h (slightly more than 5 days) in the future.

A particular time in the future can ultimately have several forecasts associated with it. For example, the 120-h forecast made on day N for five days in the future is for the same time as the 96-hr forecast made on day $N + 1$, the 72-h forecast made on day $N + 2$, the 48-h forecast made on day $N + 3$, and the 24-h forecast made on day $N + 4$. Hopefully, as day follows day, these forecasts will converge on the real meteorological condition of the atmosphere. For times significantly farther out than five days, it is likely that long-term monthly statistics will yield better results than would the individual forecasts.

Each forecast consists of surface temperature, pressure, dewpoint, and absolute humidity (of water vapor), in addition to the upper air values. Above the surface, the height, temperature, absolute humidity, and liquid water content of any clouds (if present) are given for specific pressure levels ranging from 850 mbar to 100 mbar, at 25-mbar intervals. For Goldstone, a pressure level of 850 mbar guarantees that this level will be above the surface under all atmospheric conditions. Typically, the 850-mbar level will be about 0.5 km above the surface at Goldstone (elevation approximately 1 km above sea level). For computational purposes a final (top) pressure level of 0 mbar is created, 10 km above the height of the 100-mbar level, which is approximately 15 km above the surface. Thus, there are a total of 33 pressure levels in the atmosphere model (including the surface) which create a total of 32 layers in the atmosphere. Near the surface, the layers are about 0.25 km thick, and near the top of the atmosphere, they are about 1 km thick.

Additionally, qualitative descriptions of sky cover are given. These are CLR (clear sky, 0/8 cloud cover), FEW (few clouds, 1/8 to 2/8 cloud cover), SCT (scattered clouds,

3/8 to 4/8 cloud cover), BKN (broken sky cover, 5/8 to 7/8 cloud cover), and OVC (overcast sky, 8/8 cloud cover). At this point of the forecast project, there has been no attempt to use this qualitative information in the computation of cloud effects. When more than one cloud layer is predicted, as seen either in the cloud layer descriptions (base and top heights of up to three layers) or by observation of the liquid water contents at the various levels, it is assumed that the clouds in *each* layer are present in the ground antenna beam, even if each layer is described only as FEW or SCT. An OVC description does not mean that all layers have 8/8 coverage, just that at least one of the layers has 8/8 coverage. It is likely, then, that the computations of cloud effects overestimate the presence of clouds. If quantitative values for sky coverage of each layer were available, it would be possible to statistically describe the cloud effects over the 6-h forecast period. There are eight possible permutations of clouds in three layers; but unfortunately the forecast detail at this time does not distinguish among the coverages of each individual cloud layer.

For each layer in the atmosphere, an average temperature, pressure, absolute humidity, and liquid water content is calculated from the values at the bottom and top of the layer. Cloud liquid water can still exist at temperatures substantially below 0 °C, so temperature alone is not a good indicator of cloud liquid water. For heights above 6–7 km above the surface, the clouds typically consist of ice crystals (cirrus clouds), which do not contribute to atmospheric attenuation and noise temperature. The qualitative sky condition descriptions (e.g., SCT) include the presence of these clouds, even if no clouds containing liquid water are present.

For each layer in the atmosphere (the constituents of which are oxygen, water vapor, clouds, and rain), a calculation of its total specific attenuation (in decibels per kilometer) can be made as a function of the temperature, pressure, absolute humidity, liquid water content, and rain rate (with an assumption of rain height above the surface). From the specific attenuation and thickness of each layer, the noise temperature contribution of that layer can be calculated, knowing the average physical temperature of the layer. Equations for calculating specific attenuations of oxygen, water vapor, and clouds were taken primarily from Ulaby *et al.* [7] with slight modifications and are not restated here. The rain attenuation model is based on Olsen *et al.* [8].

The total attenuation of each layer A_{total} is the sum of the specific attenuations of each constituent, multiplied by the thickness of the layer (if the ray path is vertical) or multiplied by the slant path length through the layer. A flat-Earth model is assumed, and this is sufficiently accurate for any elevation angle above 10°. The total attenuation of the atmosphere is the sum of the attenuations of all layers along the slant path. The noise temperature contribution of a layer is proportional to its attenuation and physical temperature, thus

$$T_{\text{layer}} = T_p \left(1 - \frac{1}{L} \right).$$

T_{layer} has units of Kelvins, T_p is the average physical temperature of the layer in Kelvins, and L is the dimension-

³<http://www.srh.noaa.gov/smg>

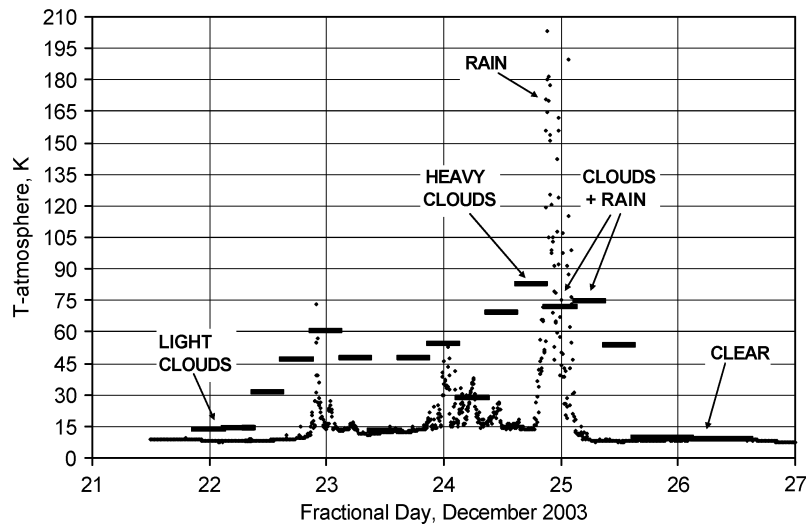


Fig. 8. Goldstone forecasted atmospheric noise temperatures and measured WVR values, December 2003.

less loss factor of the layer related to the loss A_{total} (dB) as $L = 10^{(A_{\text{total}}/10)}$, $L \geq 1$.

The effective noise contribution of each layer is the noise of that layer reduced by the attenuation of all the layers between it and the receiving antenna on the ground along a slant path at the elevation angle of interest, thus

$$T_{\text{effective}} = \frac{T_{\text{layer}}}{L_{\text{path}}} \text{ K}$$

where L_{path} is the loss factor from emitting layer to antenna, along the slant path.

The total noise contribution of the atmosphere is, thus, the sum of the effective noise contributions of the 32 layers in the predicted atmosphere profile. This computational method is called radiative transfer and is described in somewhat more detail in [9].

Fig. 8 shows a plot of forecasted zenith noise temperatures during a cloudy/rainy period at Goldstone in December 2003 (horizontal solid lines). Also shown are actual atmospheric noise temperature measurements made at the antenna site with a water vapor radiometer (WVR) at a frequency of 31.4 GHz, very close to the DSN operational *Ka*-band downlink frequency of 32 GHz (dotted curve). The forecasted noise temperatures were also calculated for the same frequency. Fractional day of the month is the elapsed time since 00Z on the first calendar day of the month; thus, fractional day 24.500 is 12Z on the 25th.

It is seen in the figure that the clear and light cloud portions of the forecasts, both at the beginning and end of the forecast period, agree reasonably well with measurements. However, the other forecasts clearly overpredict the noise temperature. Possible reasons for this were discussed earlier in this section. The “spiky” regions are likely rain events and by their very nature are difficult to predict, although for the two events near fractional days 23.0 and 24.0, the predictions are remarkably close to what was actually measured. The very large noise temperatures at day 25.0 are likely due

to water on the WVR instrument itself, rather than solely due to rain in the atmosphere.

The typical procedure in the DSN has been to assume a conservative weather model, e.g., an atmospheric noise temperature cumulative distribution value of 90%. For the Goldstone yearly average, this value at zenith is 15.1 K.⁴ If a telecommunications link were designed to have zero margin using this value, it is seen in Fig. 8 that the link would have had a slightly positive margin for those periods which were clear or contained light clouds, but would have failed for all times when the noise temperature exceeded 15.1 K, or for a period of about two days, from about day 22.9 to day 25.2, except for about 12 h at approximately day 23.5. If, on the other hand, the link used the forecasted noise temperatures, positive margin would have been maintained at all times, except for brief periods at day 23.0 and 24.0, and for several hours around day 25.0.

Present plans for using forecasts will not rely on the exact predicted number calculated by the noise temperature program, but will use that calculated number to point toward a distribution of noise temperature values determined from historical measurements made by the WVR at the same location. Several years of forecasts and measured noise temperatures have been accumulated, and for each 6-h period having a constant predicted value, a range of actual noise temperatures was measured. Typically, when clear weather has been predicted, the weather has actually been clear, and the WVR measurements have had a small range of values, with a few larger values corresponding to those times when clouds have actually been present. When forecasts of cloudy weather were made, the WVR typically measured elevated noise temperatures; however, the range of measurements was much larger, ranging from low values (where clouds were not present or the WVR was looking between clouds) to high values where a large amount of cloudiness was present, even

⁴<http://deepspace.jpl.nasa.gov/dsndocs/810-005/>

including rain events. Thus, in order to use these distributions, the historical distribution of forecasted values was divided into 5%-sized bins (5% of the forecasts were in each bin, ranging from lowest to highest), and the distribution of matching WVR measurements was calculated for each of the 6-h forecasts in each bin. Thus, if a forecast of 23.5 K were made, for example, it would fall in the 14th 5% bin of forecasts (those ranging from 22.9 K to 29.8 K). In the corresponding distribution of WVR measurements, one could then choose to use a conservative value of noise temperature (e.g. 90% CDF), a median value (e.g., 50% CDF), or an optimistic value (e.g., 25% CDF). The refinement of this technique is currently being investigated, and its success will depend on obtaining a large historical collection of forecasts and corresponding measured WVR values.

B. Link Management Based on Forecasting

Due to Earth's rotation, a DSN station views a deep space target for some period every 24 h. This observation opportunity is called a pass. Formally, a pass is defined as the event when the path elevation angle is above a minimum threshold. The duration of a pass depends on path geometry and can typically vary from a few hours up to about 14 h. If all three DSN complexes are assigned for tracking a deep space target, the nearly equally spaced locations (longitudinally) on Earth allow for near-continuous tracking of the target.

Because weather forecasts are perishable, forecasting-based link management cannot use background sequencing to command the spacecraft. It has been determined that atmospheric noise temperature predictions become somewhat inaccurate beyond five days, and they are best used within a period not exceeding three days.⁵ Hence, it is desirable to command the deep space probe as soon as a prediction becomes available. The objective is to minimize the time between when a forecast becomes available and the time that the forecast is put to use. Therefore, contingent on the mission constraints, it is recommended that when a forecast becomes available, it should be sent up to the probe at the first available opportunity. As a matter of practicality, one opportunity per day for commanding a spacecraft can be recommended.

In general, it is neither practical nor constructive to set the weather margin via controlling the radiated power of the deep space probe. There are several ways of realizing the desired margin, including (but not limited to) the appropriate selection of the following parameters: transmission rate (bit rate), coding strategy, and the carrier modulation index. Although all the above options are valid for dealing with the weather margin, the bit rate is the most useful one. Lowering the bit rate allows more energy per bit to be transmitted, thus increasing the link margin. Simply, the probe will transmit more data during good weather periods and will transmit less data during bad weather periods. Therefore, in response to a weather forecast, the desired rate profile is uplinked to the

probe. In practice, the bit-rate profile must comply with certain constraints, including the selection of the bit rate from a limited number of choices permitted by the deep space transmitter. This idea is expanded in the next section.

VII. MRO KA-BAND LINK DESIGN AND PERFORMANCE PREDICTIONS

The purpose of this section is to provide a quantitative evaluation of the link prediction methods discussed in this paper and to present specific test cases to be demonstrated by the MRO spacecraft. Sections IV, V, and VI presented the annual statistics of the G/T, monthly statistics of the G/T, and the forecasting of the G/T as means of determining the transmission data rate.

In this section, the *Ka*-band link is designed to maximize the average data return over the pass subject to a minimum availability constraint. The mathematical formulation of this approach has been outlined in several papers previously [10]–[12] and, therefore, is not discussed here. Different methods of designing the link are briefly introduced. Then the performance of each method for MRO using monthly statistics is evaluated. Finally, using illustrative examples, the performance of the link when monthly or forecast statistics are used is compared to that of the link when yearly aggregate statistics are employed. Increased data volume, increased availability, or both are the desired measures.

A. Link Design Methods

While recognizing MRO constraints, four different design methods are considered for use for the MRO *Ka*-band demonstration.

- 1) Multirate 0 (MR-0): The link is designed with as many data rate changes as necessary to maximize data return. No restrictions are placed on the minimum availability. This method will return, on the average, the maximum amount of data.
- 2) Multirate 90 (MR-90): This method is the same as MR-0, except the availability of the link has to be greater than 90% for each pass.
- 3) Dual-rate 90 (DR-90): With this method the number of data rates is limited to two. Under this constraint, the average data return is maximized subject to a minimum of 90% availability for each pass.
- 4) Single-rate 90 (SR-90): With this method, only a single data rate could be used during the pass. Therefore, a single data rate is selected to maximize the average data return subject to a minimum of 90% availability for each pass.

Given the data rates, coding capabilities, distance, and declination of MRO during its projected two-year primary mission, the above methods were applied to the period from December 2006 through November 2008 to calculate the optimum *Ka*-band data rate profiles for the mission and to obtain estimates for the expected data return over a pass during this period. For these calculations aggregate monthly statistics were used. For this analysis, occultation was ignored, as the occultation periods of the spacecraft

⁵http://www.weather2000.com/faq/faq_integrity.html;
<http://www.ametsoc.org/policy/statewaf.html>

Mars Declination and Maximum Elevation for Different Site vs. Time, MRO Ka-band Experiment

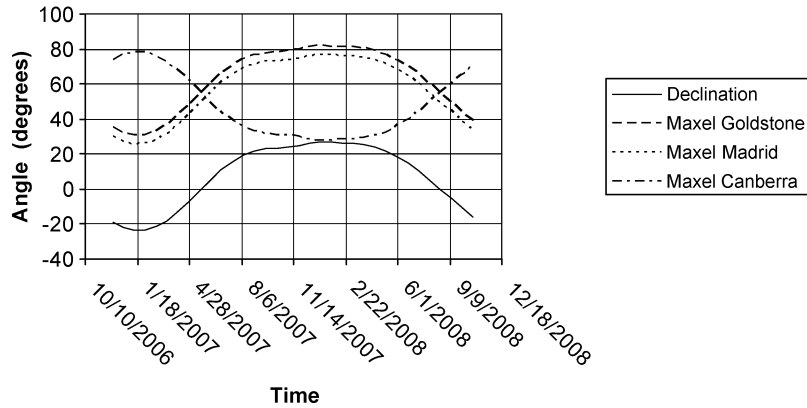


Fig. 9. Mars declination and maximum elevation as viewed from DSN antenna locations during MRO *Ka*-band demonstration. Maxel: maximum elevation.

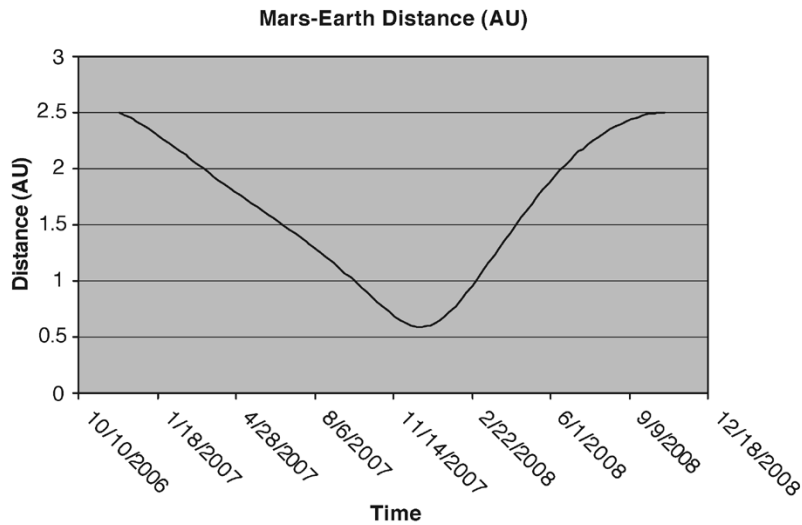
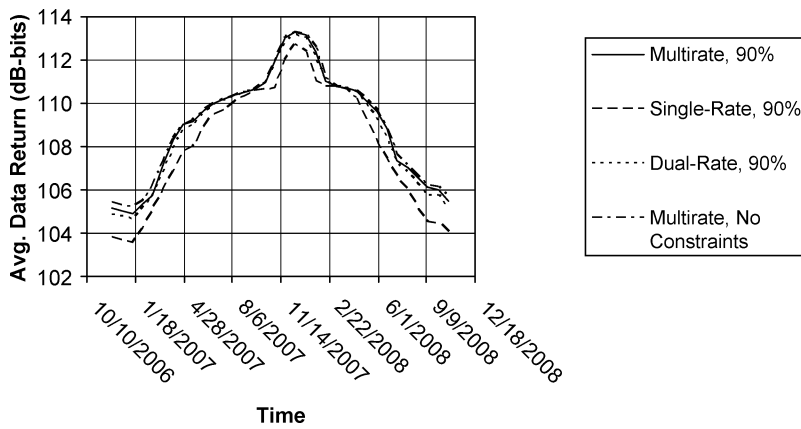


Fig. 10. Mars–Earth distance for the period of interest.

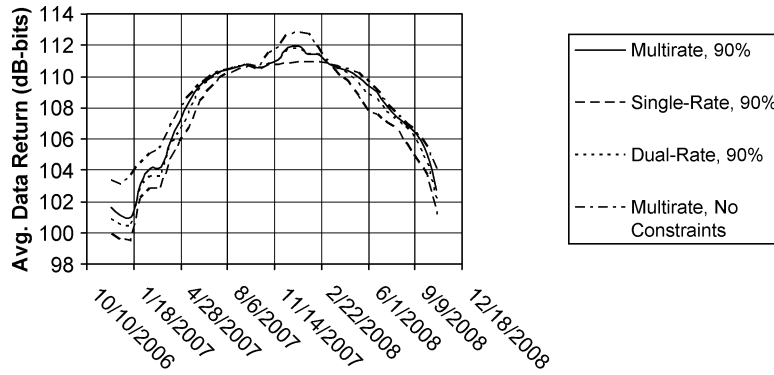
are dependent on the exact arrival and Mars orbit insertion process during the actual mission.

Fig. 9 shows Mars declination during the period under consideration along with the maximum elevation observed at each DSN complex. Note that negative Mars declination angles yield larger path elevation angles at Canberra, the site in the southern hemisphere, than at the other two complexes. In Fig. 10, the distance of the spacecraft from Earth is plotted in astronomical units (AU) where an astronomical unit is the mean distance of Earth from the sun, 149 598 000 km. Fig. 11(a)–(c) shows the expected data return during the period under consideration for the different methods at Goldstone, Madrid, and Canberra, respectively. Fig. 12(a)–(c) shows the average link availability. As seen from these figures, among the methods under consideration, MR-0 returns the most amount of data, and SR-90 returns the least amount of data. Conversely, SR-90 has the highest average availability, while MR-0 has the lowest. This is due the fact that for the single data rate case as the elevation increases so does the reliability of the link. A single low-data rate is set to allow communication at low elevation angles

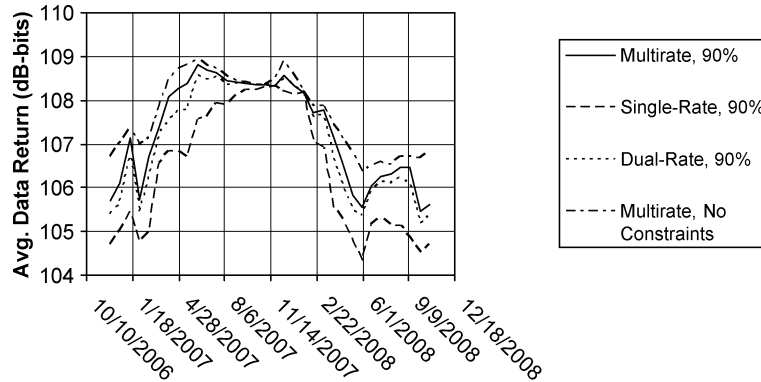
where G/T is significantly lower than at meridian crossing, at a high-elevation angle. However, for multiple-rate cases, since the data rate changes as a function of elevation (the higher the elevation, the higher the data rate) the reliability does not increase significantly as the elevation increases. Furthermore, note that while the MR-90 method returns almost as much data as MR-0 for Goldstone, it returns significantly less data on the average than MR-0 for Madrid and Canberra. This is due to the fact that the optimum *Ka*-band weather to maximize data volume for Goldstone is usually around 90%, while the optimum *Ka*-band weather for the other sites is between 70% and 90%, depending on the time of the year and elevation. Finally, note that for MRO, there is very little difference in the performance of MR-90 and DR-90 methods in terms of data return due to the limited number of allowable data rates—see Table 1. However, for a different spacecraft with a finer set of allowable data rates, MR-90 performance is likely to noticeably exceed that of DR90. This indicates that using at most two data rates may be sufficient for returning data on *Ka*-band from MRO.



(a)



(b)



(c)

Fig. 11. Expected data return during the period of interest at (a) Goldstone; (b) Madrid; and (c) Canberra, employing monthly statistics.

B. Monthly Variations

In Section VII-A, monthly variations were used to calculate the optimum data rate profiles subject to various data rate changes and availability constraints. In order to illustrate the advantages of using monthly statistics over yearly statistics, MR-90 methodology was applied to an MRO-type spacecraft at a distance of 2.4 AU with a declination of 0° , tracked with a 34-m BWG antenna at the three DSN sites for different months. First, using aggregate annual statistics, the optimum data rate profile was calculated for the elevation profiles at each site. Then this data rate profile was used in conjunction

with monthly atmospheric noise temperature statistics to calculate the average data return and the average availability for the data rate profile for each month. Finally, the results were compared to those obtained by using monthly optimized data rate profiles for each month. The results of this analysis are shown in Fig. 13(a)–(c).

These figures indicate that the expected data return over the link varies from month to month. When the link is optimized according to the monthly statistics, this variation is more pronounced. Also note that while sometimes the average data return is higher for the yearly optimized

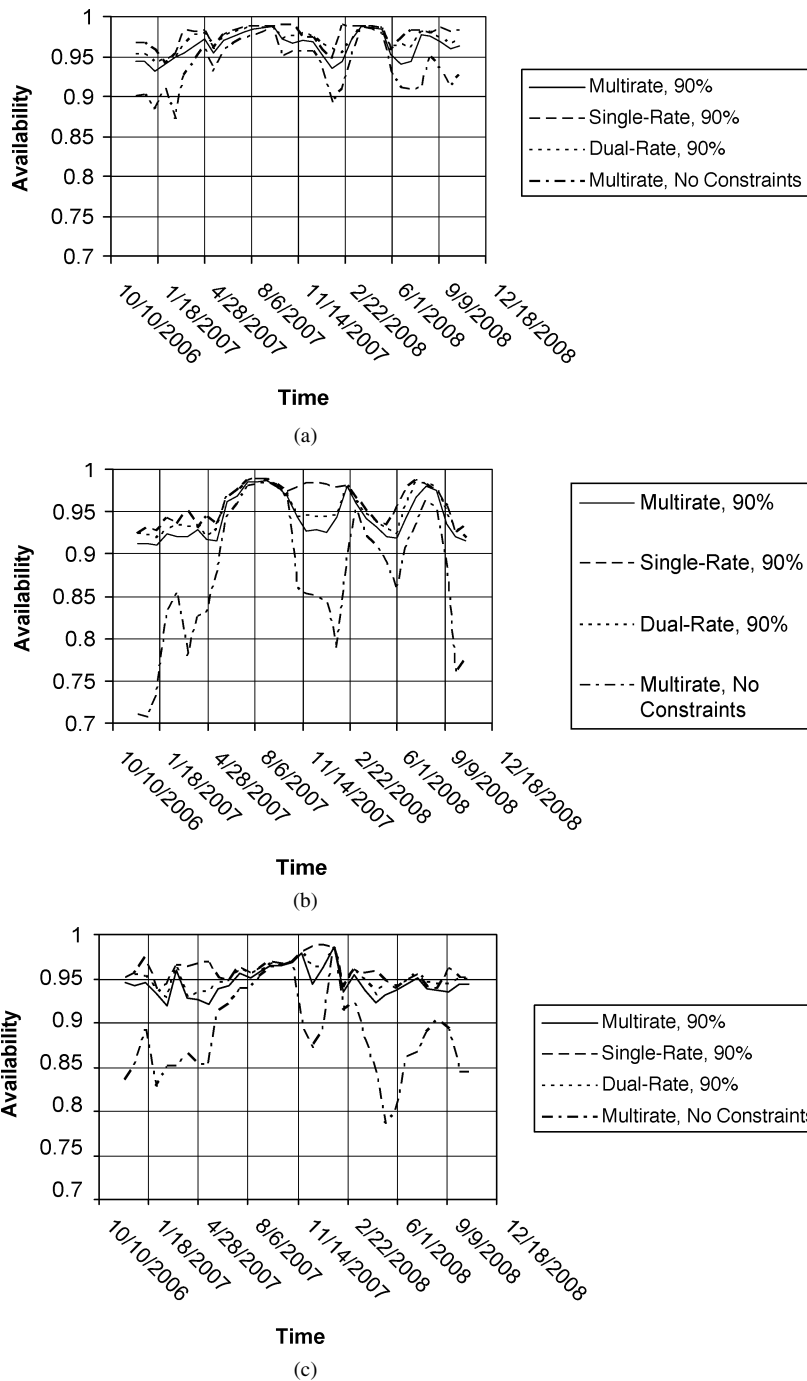


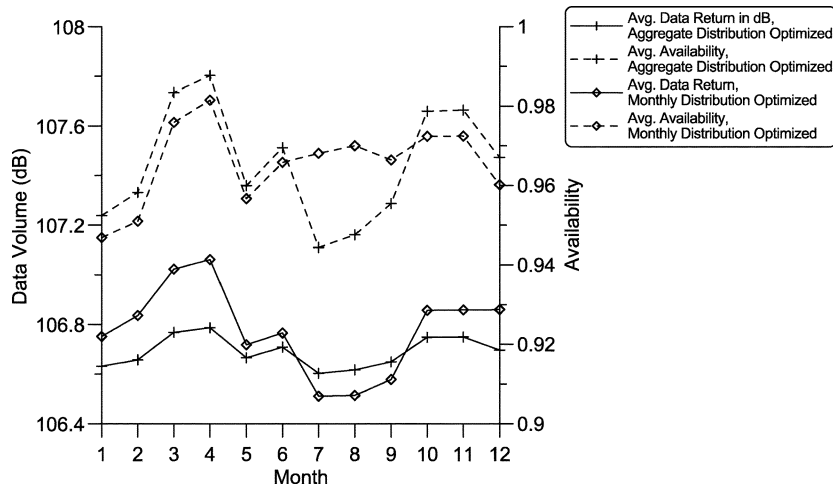
Fig. 12. Average link availability during the period of interest at (a) Goldstone; (b) Madrid; and (c) Canberra, employing monthly statistics.

Table 1
Assumed MRO Allowable Data Rates

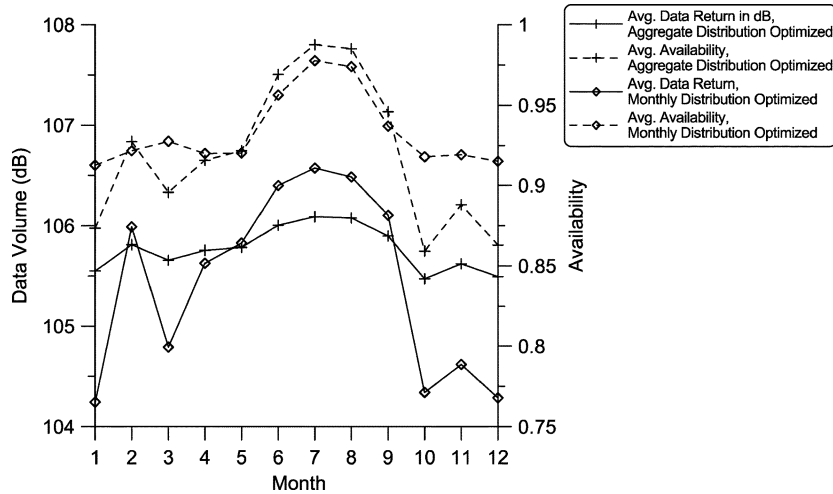
bps	34.38	80	160	400	1000				
kbits	2	32	64	125	200	350	500	600	800
Mbps	1.0	1.5	2.0	2.25	2.6	3.0	3.5	4.0	5.0

data rate profile, in those cases the average availability is lower; at times, significantly so. This indicates that using the yearly optimized data rate profile does not meet the minimum 90% availability requirement for that month. On the other hand, when the average data return for the

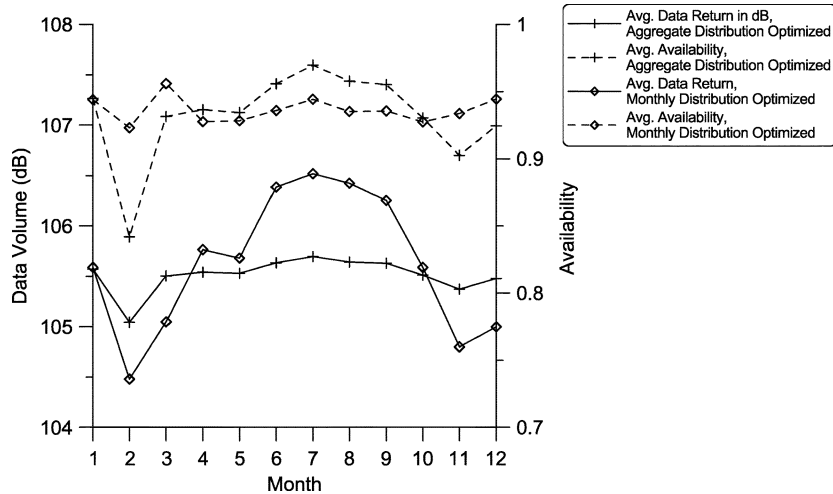
monthly optimized link is greater than that for the yearly optimized link, the link's average availability is only slightly less than that for the yearly optimized link, while the data return for the monthly optimized link could be significantly higher.



(a)



(b)



(c)

Fig. 13. Monthly average data return and average availability using multiple data rate optimization (MR-90) with the constraint of minimum 90% availability. (a) Goldstone. (b) Madrid. (c) Canberra.

It could also be concluded from Fig. 13(a)–(c) that the use of seasonal models for Ka -band is more important for the overseas sites than it is for Goldstone. These figures indicate that the greatest monthly variation occurs in Madrid with a

significant difference in data return (about 2 dB) and link availability (about 6%) between the summer months (from June through September) and the autumn and early winter months (from October through January). Fig. 13(c) indicates

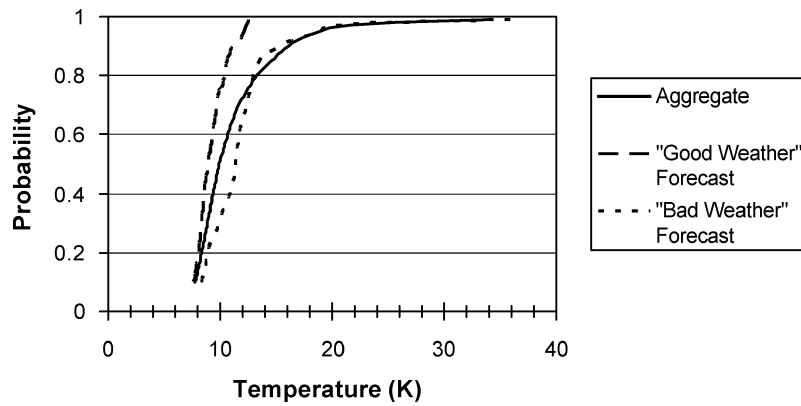


Fig. 14. Zenith atmospheric noise temperature distribution, aggregate and forecast, Goldstone.

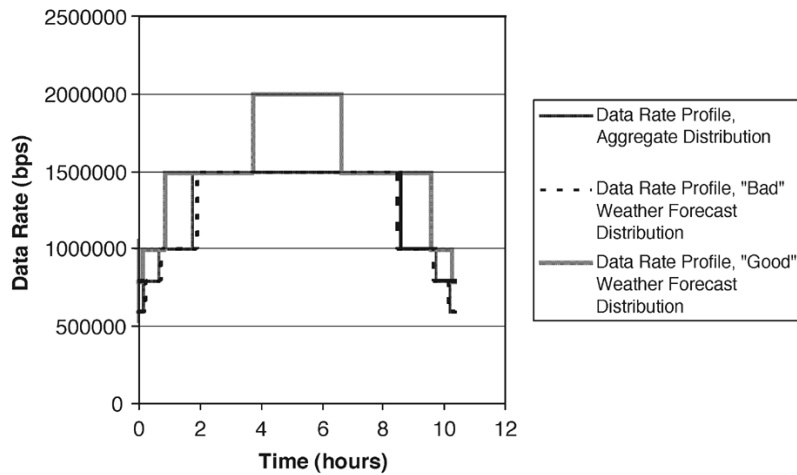


Fig. 15. MR-90 data rate profile for different zenith noise temperature distributions for an MRO-type spacecraft at Goldstone, 0° declination, 2.4 AU distance.

that Canberra has roughly two seasons, with the period of relatively good weather lasting from April through September and the period of relatively bad weather starting in October and ending in March. Fig. 13(a) indicates that compared to the other DSN sites, Goldstone has relatively little seasonal variation, with the summer months (July–September) having slightly worse, and late winter/early spring months having slightly better performance than the average.

C. Forecasting

As was indicated in Section VI, the link forecasting algorithm will generate atmospheric noise temperature distributions that could be used in conjunction with the link design methods presented above. In order to illustrate the effects of forecasting on the link performance, two forecast distributions along with the annual aggregate distribution for Goldstone were used in conjunction with MR-90 link design algorithm to evaluate the performance of the link for an MRO-type spacecraft at a distance of 2.4 AU and a declination of 0° .

Fig. 14 shows the distributions. The two forecast distributions were obtained as part of the development of the forecasting algorithm for Goldstone. As there are comparatively few forecasts available, these distributions are not as smooth

as the aggregate distribution. Compared to the aggregate distribution, the “good” weather forecast distribution has a very small span (less than 3.5 K) and in general has low values (less than 11 K). The “bad” weather forecast distribution has generally higher temperature values than the aggregate distribution, but at higher percentage values of weather (above 90%), it is almost identical to the aggregate distribution. Note that because of the relatively small amounts of data used to generate forecast distributions, the “bad” weather forecast distribution actually indicates a lower zenith noise temperature value for weather between 76% and 88% weather than does the aggregate distribution. This apparent anomaly is caused by statistical noise.

Applying the MR-90 algorithm to the distributions in Fig. 14, the data rate profiles in Fig. 15 were obtained for a pass lasting about 10 h. As expected, when a “good” weather forecast distribution is used, the link can support much higher data rates and, thus, return more data. In addition, note that MR-90 data rate profiles for the aggregate distribution and the “bad” weather forecast distribution are almost identical. This is to be expected, as the two distributions are almost identical for weather values above 90%.

Finally, the average data return and the availabilities for when the forecast distributions apply to the pass are shown

Table 2

Data Return and Average Availability for Different Forecast Distributions and Data Rate Profiles

Distribution	Avg. Data Volume, Forecasting	Avg. Availability, Forecasting	Avg. Data Volume, Aggregate Statistics	Avg. Availability, Aggregate Statistics
"Good" Weather Forecast	107.51 dB-bits	0.980	106.84 dB-bits	1.000
"Bad" Weather Forecast	106.65 dB-bits	0.968	106.63 dB-bits	0.952

in Table 2. This table provides a comparison between the average amount of data returned by an MR-90 data rate profile obtained specifically for the forecasted distribution and an MR-90 data rate profile obtained from the aggregate distribution. As expected, when the "good" weather forecast distribution applies, the average data return is improved, by about 0.7 dB, by using forecasting. However, the performance of the link is similar for both data rate profiles when a "bad" weather forecast distribution applies during the pass. This is again due to the fact that the aggregate distribution data rate profile for the pass is very similar to the "bad" weather forecast distribution data rate profile.

Since Goldstone has a dry climate, the performance difference between employing forecasting versus using aggregate annual statistics is not as large as it would be for a region having a wetter climate. At this time, forecast data from the other two sites, Madrid and Canberra, were not available. It is expected, however, that when forecasting is applied to these sites, a bigger improvement will be observed.

VIII. SUMMARY

The DSN uses radio frequency signals to communicate with deep space probes (spacecraft). In the near future, the DSN will make a transition from the *X*-band region of the radio spectrum to the *Ka*-band region to improve communications and navigation capabilities. The MRO spacecraft, scheduled for launch in August 2005, will be used as a test bed to demonstrate the operational use of the *Ka*-band for deep space applications.

Due to the increased atmospheric losses associated with *Ka*-band, novel link management techniques are required to fully benefit from the use of *Ka*-band. Three link management approaches were discussed in this paper.

- 1) The atmospheric margin is calculated from the aggregate annual statistics of the site of interest for a desired long-term availability level.
- 2) The seasonal statistics of the site of interest are used in lieu of the annual statistics.
- 3) Weather forecasting can be used to predict the atmospheric margin of the site of interest for a desired availability level

The first option is not recommended for *Ka*-band links because it does not address the impact of the seasonal variability of the weather on the link budget. The second option is shown to be more effective by taking advantage of seasonal variability of the weather to improve performance. Option 2) is also shown to be simple to operate by using back-

ground sequencing to command the deep space probe only once per month. Option 3) is shown to have the most potential for improving link performance at the cost of a moderate increase in complexity. With this option, background sequencing is replaced with a command scheme that allows more frequent updates. Option 3) also requires the services of a weather organization, public or commercial, to routinely provide weather forecasts on a daily basis. Furthermore, it was shown that for all three options performance improves by changing the data rate during a pass.

The findings of the MRO demonstration will be disseminated via a publication in 2009.

ACKNOWLEDGMENT

The authors would like to thank the Systems Engineering Office of the Jet Propulsion Laboratory's (JPL's) Interplanetary Network Directorate for support of the work described in this paper. The authors would also like to thank JPL's MRO Project for its commitment to provide the deep space link opportunity for testing the methodologies developed in this paper. The authors would also like to thank the NOAA National Weather Service Spaceflight Meteorology Group, Johnson Space Center, Houston, TX, for doing an excellent job in providing daily weather forecasts for the Goldstone Deep Space Communications Complex.

REFERENCES

- [1] G. Noreen *et al.*, "Telecommunications systems evolution for Mars exploration," presented at the 54th Int. Astronautical Congr. Int. Astronautical Federation, Int. Academy of Astronautics, and Int. Institute of Space Law, Bremen, Germany, 2003.
- [2] "Propagation data and prediction methods required for Earth-space telecommunication systems," Int. Telecommun. Union, Geneva, Switzerland, ITU-R Recommendation P.618-8, Apr. 2003.
- [3] *Proc. IEEE (Special Issue on Ka-Band Propagation Effects on Earth-Satellite Links)*, vol. 85, pp. 805-1024, June 1997.
- [4] *Radio Regulations*. Geneva, Switzerland: Int. Telecommun. Union, 2001, pp. RR5-85-RR5-107.
- [5] M. D. Johnston *et al.*, "Overview of Mars reconnaissance orbiter mission," presented at the 2003 IEEE Aerospace Conf., Big Sky, MT, 2003.
- [6] J. Berner *et al.*, "Dynamic telemetry bit rates for deep-space communications," presented at the 2001 IEEE Aerospace Conf., Big Sky, MT, 2001.
- [7] F. T. Ulaby, R. K. Moore, and A. K. Fung, *Microwave Remote Sensing, Active and Passive*. Reading, MA: Addison-Wesley, 1981, vol. 1.
- [8] R. L. Olsen, D. V. Rogers, and D. B. Hodge, "The aR^b relation in the calculation of rain attenuation," *IEEE Trans. Antennas Propagat.*, vol. AP-26, pp. 318-329, Mar. 1978.
- [9] S. D. Slobin, "Microwave noise temperature and attenuation of clouds: statistics of these effects at various sites in the United States, Alaska, and Hawaii," *Radio Sci.*, vol. 17, no. 6, pp. 1443-1454, Nov.-Dec. 1982.

- [10] S. Shambayati. (2002, Feb.) Maximization of data return at X-band and Ka-band on the DSN's 34-meter beam-waveguide antennas. *Interplanetary Netw. Prog. Rep.* [Online]. Available: http://ipnpr.jpl.nasa.gov/tmo/progress_report/42-148/148E.pdf
- [11] —, (2003, Aug.) On the use of W-band for deep-space communications. *Interplanetary Netw. Prog. Rep.* [Online]. Available: http://ipnpr.jpl.nasa.gov/tmo/progress_report/42-154/154E.pdf
- [12] —, "On the benefits of short-term weather forecasting for Ka-band (32 GHz)," presented at the IEEE Aerospace Conf., Big Sky, MT, 2004.



Faramaz Davarian received the Ph.D. degree in electrical engineering from the University of Southern California, Los Angeles, in 1975.

He joined the Jet Propulsion Laboratory (JPL), Pasadena, CA, in 1982 to work on the Mobile Satellite Experiment (MSAT-X). During his participation in that project from 1982 to 1986, he made many contributions to the development of mobile satellite technologies. From 1987 to 1996, he supervised the Spectrum Engineering Group and managed the NASA Propagation Program at

JPL. In 1996, he joined Hughes Space and Communications Company, El Segundo, CA, as the Chief Technologist in the Processing Payload Business Unit, where he contributed to a number of satellite-based programs, which included mobile, direct broadcast, and high bit-rate applications. From 2001 to 2002, he was Head of the Systems Engineering Department at Sirius Satellite Radio, New York, focusing on the development of satellite radio technologies. In 2003, he rejoined the Jet Propulsion Laboratory, where he is currently the Principal Investigator of the Mars Reconnaissance Orbiter Ka-Band Demonstration. Since 1986, he has also been a Part-Time Faculty Member of the engineering department of Loyola Marymount University (LMU), Los Angeles, where he teaches graduate-level courses in communications.



Shervin Shambayati received the B.S. degree in applied mathematics and engineering from California State University, Northridge, in 1989 and the M.S.E.E., Engineer's, and Ph.D. degrees from the University of California, Los Angeles, in 1991, 1993, and 2002, respectively.

In 1993, he joined the Deep Space Communications Systems Group at the Jet Propulsion Laboratory (JPL), Pasadena, CA, where he took part in the development and testing of Deep Space Network's Galileo Telemetry receiver (DGT). In 1997, he joined the Information Processing Group at JPL, where he has been involved in various projects, including the Mars Global Surveyor's Ka-Band Link Experiment II, Deep Space 1 Ka-band testing, and the 70-m antenna Ka-band Task. His current research interests and activities include evaluating the effects of weather outages on spacecraft resources, Ka-band weather forecasting, Ka-band link designs for the Mars Reconnaissance Orbiter and Mars Telecommunication Orbiter, and engineering support for implementation of Ka-band services in NASA's Deep Space Network.



Stephen Slobin received the B.S. degree in electrical engineering from the California Institute of Technology, Pasadena, in 1961, and the M.S. and Ph.D. degrees in electrical engineering from the University of Southern California, Los Angeles, in 1963 and 1969, respectively.

From 1969 to 1970, he was with TRW Systems Group, Redondo Beach, CA, where he worked in the area of remote sensing. From 1972 to 1974, he was with Aerojet ElectroSystems Company, Azusa, CA, where he carried out antenna analysis and radar meteorology studies. Since 1975, he has been with the Jet Propulsion Laboratory, Pasadena, where he has been involved in gain, noise temperature, and pointing calibration of the NASA Deep Space Network (DSN) antennas and has developed weather effects models for use in telecommunications link design. He has recently been working on the development of a telecommunications weather-effects prediction methodology using forecasts provided by the National Weather Service for the DSN antenna locations. The first use of this new prediction technique will be in support of the Mars Reconnaissance Orbiter Mission in 2005.